STRUCTURAL ANALYSIS OF EXPERIMENTAL CARBIDE FUELED DRIVER ASSEMBLY FLOW DUCT FOR TESTING IN THE FFTF

G. H. ROWE, D. D. MEHTA, W. E. DESAULNIERS

Fast Breeder Reactor Engineering Development, C-E Power Systems, Combustion Engineering Inc., 1000 Prospect Hill Road, Windsor, Connecticut 06095, U.S.A.

SUMMARY

Mixed carbide fueled driver assembly experiments will be tested in FFTF fuel driver positions as part of the National Advanced Fuel Program. The design of the experimental flow ducts must assure conformance to FFTF functional requirements in addition to service as a test vehicle for the carbide fuel irradiations. Test goals of damage fluence, burnup, and fluence to burnup ratio exceed those of the standard oxide fueled drivers. As a consequence, the 20% cold worked type 316 stainless steel material of construction will experience significant irradiation induced creep and swelling. Additionally, the flow duct design must withstand the enhanced thermal transients produced by the action of carbide fuel during reactor scrams.

A major FFTF functional requirement is that adjacent flow ducts do not touch each other except at the load pads. This requires a realistic analysis of the creep and swelling deformation of the flow duct during an experiment lifetime. Flow duct dilation, i.e., diametrical growth of the hexagonal cross section, was investigated by the MARC-CDC finite element program. Subroutines for irradiation creep and swelling were incorporated into the program. The model for the 2-D duct dilation analysis was a transverse slice through one-half of one hexagonal cross section flat (midflat to corner). The ends were free to slide outward. Generalized plane strain modelling was required to satisfy boundary conditions and high stress gradients in the corner. Mesh optimization showed that a second order, ten node, distorted quadrilateral element was preferred to a simpler first order, six node, isoparametric quadrilateral element. The former, while requiring a large computer storage space, permitted a rather coarse mesh. The latter would have required an uneconomical, extremely fine mesh at the corner. Maximum flow duct dilation occurs between opposing hex flats at about three-quarters of the enriched core height, an axial position where neutron flux, temperature, and pressure collectively have the greatest effect on creep and swelling. After an incubation period, the dilation increases linearly with damage fluence.

A simple analytical procedure for maximum dilation was also developed. The formulation for elastic deformation of a beam with fixed ends and uniform load was modified to include a creep modulus and a swelling expression. Midflat dilation at one-inch intervals along the axis of the active core and the axial position of maximum dilation agreed reasonably with MARC-CDC results.

The Above Core Load Pad of the flow duct was stress analyzed for rupture and creep-fatigue failure modes under carbide fuel thermal transient, core restraint, and seismic loadings. The analytical results for dilation indicate that carbide fueled experimental flow ducts must be reduced in diameter sufficiently to provide an enlarged gap to accommodate the increased flow duct dilation. However, the resulting increased Above Core Load Pad thickness leads to concern in being able to satisfy the creep-fatigue failure criterion.

1. Introduction

An expedient means for testing advanced carbide LMFBR fuels is to substitute carbide fuel test assemblies for selected standard oxide fuel assemblies in the Fast Test Reactor (FTR) of the Fast Flux Test Facility (FFTF) [1]. Conditions prototypic of CRBR and commercial LMFBR's can be achieved by judicious selection of test location (row, position) and design of the test assemblies with respect to physical configuration of the pin bundle and duct, fuel fissile plutonium enrichment, and linear power-to-sodium coolant flow ratio. Prototypic conditions to be simulated include power, pressure, drop, coolant velocity, cladding temperatures, burnup, and fluence-to-burnup ratio. While, in part, the design of a carbide fuel test assembly must satisfy National Advanced Fuels Program test objectives, the design must also simultaneously satisfy FFTF functional requirements for an FTR fuel assembly [2,3]. Therefore, it was the purpose of this study to analyze the suitability of the standard oxide fuel flow duct (with and without minor modifications) for use in the carbide fuel test assemblies.

Advanced Fuels Program test goals for burnup, damage fluence, and fluence-to-burnup ratio in the FTR tests exceed those of the standard FTR oxide fuel assemblies. For this reason, the 20% cold-worked 316 stainless steel flow duct will experience significant irradiation induced creep and swelling deformation. A major FFTF functional requirement is that adjacent flow ducts do not touch each other except at the load pads. This requirement implies that flow duct dilation, i.e., diametrical growth of the hexagonal cross section, must be limited to less than one-half the interduct spacing. Otherwise, excessive dilation would create interference with the above core load pads of adjacent assemblies during removal of the assembly from the core. Permanent bowing creates curvature of the assembly, but was not included in this analysis of the flow duct deformation.

Because of the interest in flow duct dilation, a method was needed for analysis of the creep and swelling deformation of the flow duct during the lifetime of an advanced fuel experiment in FTR. It was recognized that a finite element formulation would be well suited to the task. However, in the long run, a simpler, inexpensive method would offer considerable savings. Therefore, the work conducted in this study, while based upon a finite element inelastic analysis of the flow duct, also led to the development of a simplified procedure. In this procedure, the formulation for elastic deformation of a beam with fixed ends and uniform load was modified to include an irradiation creep modulus and an irradiation swelling expression.

Because of the thermophysical characteristics of carbide fuel, a normal reactor scram event will produce an enhanced thermal transient on the test assembly as compared to that on a standard oxide fuel assembly [4]. Preliminary evaluation of the effect of the worst carbide assembly transient on the standard flow duct showed that the upper handling socket and the floating collar could withstand the transients. However, the above core load pad (ACLP) appeared to be marginal, particularly if thermal stresses were combined with stresses from core restraint and seismic loadings [5]. Therefore, detailed stress analysis and structural evaluation were performed on the ACLP of the carbide fuel test assembly flow duct [6].

2. The Standard FTR Fuel Assembly and Modifications for Carbide Fuel Irradiations

The standard FTR oxide fuel assembly is depicted in Figure 1. A one piece, hexagonal flow duct is joined at the top to the handling socket and at the bottom to the inlet/shield/orifice assembly. The fuel pin bundle is mounted on the shield/orifice piece and extends into the flow duct. The flow duct is constructed of 20% cold-worked type 316 stainless steel (CW316SS). The top and bottom end pieces are machined from solution annealed type 316

stainless steel (SA316SS). Each assembly is restrained at three locations: the inlet nozzle (core support plate), and by adjoining assemblies at the above core load pad and the top load pad. Clearance between the floating collar (top load pad) and the handling socket does permit some free lateral movement of the upper part of the assembly.

The combined effects of neutron damage fluence, temperature, and pressure upon flow duct dilation are of significance only in the thirty-six inch fuel bearing region of the assembly. Therefore, it is this region that is of interest to the dilation analyses. This region was also evaluated for possible modifications to the flow duct design to permit exposure to higher fluences without exceeding the allowable dilation limit. Three flow duct designs, the standard (MARK-IA) and two with modifications to the fuel bearing region (MARK-IB, IC), were evaluated in this study. They are described in Table I.

3. FTR Core Environment

The active core of FTR is composed of six rows with three orifice regions: rows 1 to 4, row 5, and row 6. The fuel fissile plutonium enrichment is increased in the outer rows and the sodium flow is reduced to compensate for the drop in fast neutron flux thereby maintaining the core outlet temperature. At the beginning of this study the Initial Core operating temperatures for FTR were specified as 600 F inlet and 900 F outlet (mixed mean). HEDL has recommended an 80 F increase in both temperatures. As of this writing, the recommendation has not been adopted; however, the flow duct evaluations for the carbide fuel test assemblies have been conservatively based upon the higher temperatures.

To investigate the flow duct dilation of a given test assembly over the length of its fuel bearing region, it is necessary to characterize the axial profiles of neutron damage flux, duct wall temperature, and coolant pressure differential across the duct wall. Detailed thermal hydraulic and nuclear physics studies are conducted to arrive at appropriate values for a particular test location (row, position) for a typical, representative FTR core configuration. The exact core configuration will not be known until shortly before the actual reactor operating cycle. However, the values and the way they are used in the dilation studies serve to upper bound the results.

The maximum flux level was assumed to occur at the core centerplane. The end flux levels (top and bottom of the fuel region) were specified by a core extrapolation length. The neutron damage flux axial distribution was represented by:

$$\phi(z) = \phi_{max} \sin \left[\pi \frac{(Z + e)}{(H + 2e)} \right] \qquad (1)$$

where, $\phi(z)$, ϕ_{max} = neutron damage flux at "Z" and centerplane, E >0.1 MeV

e = extrapolation length (FTR design ∿ 6.9 in.)

H = fueled height (36 in.)

Z = axial distance along the core height

Nuclear physics studies established axial and radial peaking factors of damage fluence for typical test locations (row, position).

Because of bypass flow along the duct wall, the duct runs cooler than the mixed-mean temperature of the coolant flowing through the fuel pin bundle. The ENERGY code was used to compute the temperatures of the edge flow subchannels on the hottest flat [17], and assuming an adiabatic duct wall, the average of these temperatures was taken as the wall temperature. The axial temperature profile for the duct wall over the fuel bearing region was conservatively

characterized by:

$$T_{duct} = T_{in} + \tfrac{1}{2} (T_{out} - T_{in}) \left(1 + \sin \left[\pi \frac{Z - \frac{H}{2}}{H} \right] \right) \qquad (2)$$

where, T_{in} = duct wall inlet temperature (680 F)

T_{out} = duct wall average temperature at top of fueled region, hot flat

The pressure differential across the duct wall is due to the pre-sure difference between the main sodium flow through the fuel pin region and the leakage flow between adjacent assemblies. The pressure differential varies linearly in the direction of flow from a maximum at the bottom to a minimum at the top of the core:

$$\Delta P_Z = \Delta P_{in} - (\Delta P_{in} - \Delta P_{out}) \frac{Z}{H} \qquad (3)$$

where, ΔP_Z = pressure differential at "Z"

ΔP_{in} = pressure differential at bottom of fueled region

ΔP_{out} = pressure differential at top of fueled region

Typical axial profiles of neutron damage fluence, temperature, and pressure are shown in Figure 2 for an FTR Row 4 position.

4. Irradiation Induced Creep and Swelling

Potential contributions to flow duct dilation include irradiation creep and swelling, thermal creep, elastic strain, and thermal expansion. Investigation of these parameters showed that only irradiation creep and swelling are significant. Thermal creep and elastic strain are negligible. Thermal expansion is accounted for in the design of FTR by providing the cold assemblies with a 0.015 in. clearance between adjacent ACLP's. This clearance reduces to just touching of the load pads when the reactor is at operating temperature. The interduct spacing at this temperature is 0.140 in.

The effect of irradiation induced swelling on flow duct dilation is depicted in Figure 3a. The combined effects of irradiation induced swelling and creep are depicted in Figure 3b. The swelling phenomenon occurs as a volumetric expansion. The irradiation creep phenomenon occurs as a volumetric expansion. The irradiation creep phenomenon is analogous to thermal creep except that it occurs at lower temperatures and is linearly related to stress. In the USA, design equations for irradiation induced creep and swelling of 20% CW316SS are published by HEDL in the Nuclear Systems Materials Handbook [8]. The equations are periodically revised as more information is gained from experimental test programs. During the course of this study, swelling revisions 3, 4, and 5 and creep revisions 2 and 3 were issued. The dilation analysis with MARC-CDC and the development of the simplified procedure were conducted with swelling revisions 3 and creep revision 2. Both programs were subsequently updated to the later revisions. Any attempt to describe all of these equations would be beyond the scope of this paper and the reader is referred to the Handbook for specific details. The following equations are typical of the formulations that were incorporated into the dilation analysis procedures.

Creep, Irradiation Induced (Revision 2[8])

Deviatoric Creep

$$\frac{\dot{\bar{\varepsilon}}}{\bar{\sigma}} = \frac{A}{B} \exp(-f/B)\, \dot{f} + C\dot{f} + D\dot{S}_o + C\dot{f} \qquad (4)$$

where, $\dot{\bar{\varepsilon}}$ = effective strain rate $\quad \dot{S}_o$ = stress-free swelling rate

$\bar{\sigma}$ = effective stress $\quad \dot{f}$ = fluence ($\dot{f}$ = rate), E>0.1 MeV

A, B, C, D, are coefficients

Dilatational Creep (Stress Affected Swelling)

$$\dot{S} = \dot{S}_o (1 + P\sigma_H) \tag{5}$$

where, $\dot{S}$, $\dot{S}_o$ = total and stress-free swelling rates, respectively

σ_H = hydrostatic component of stress $\quad$ P = coefficient

Stress-Free Swelling, Irradiation Induced (Revision 3[8])

$$\frac{\Delta V}{Vo} = S_o = 0.01\ R\ [\phi t + \frac{1}{\alpha}\ \text{Ln}\ [\frac{1 + \exp\ [\alpha\ (\tau - \phi\tau)]}{1 + \exp\ (\alpha\tau)}\ y] \tag{6}$$

where, ϕt = neutron fluence in units of 10^{22} n/cm^2 (E > 0.1 MeV)

R,τ,α = temperature dependent functions

These equations have upper and lower bound confidence limits. All the upper bound limits for the coefficients P, D, C and S_o were assumed to represent the nominal + 3σ confidence limit (σ being the standard error deviation). All lower bound limits were assumed to correspond to nominal -3σ. In this study, the dilation analyses were conducted at a statistical limit of nominal + 1σ; i.e., the probability of a carbide test assembly flow duct not exceeding the dilation limit is about 84%. Essentially the equations, at a given damage flux, stress and temperature, predict very low creep and swelling rates during a fluence incubation period (typically 5 to 9 x 10^{22} n/cm^2) and this is followed by significant creep and swelling rates which are constant with time.

5. C-E Simplified Procedure for Dilation Analysis

Components of dilation to be calculated include stress-free swelling, dilatational creep, and deviatoric creep. Computation of the stress-free swelling is straightforward. The empirical approach for the creep components was adopted from [9] in which it was assumed that duct rounding, which results from irradiation induced creep strain, is identical to that which would result from the same amount of elastic strain. Their model was a beam with fixed ends and uniform load, representing a transverse slice (unit width) through one side (flat) of the hexagonal flow duct cross section. For such an elastic beam of length ℓ, thickness t, and uniform pressure loading ΔP, the mid span deflection D_e is given in terms of the bending strain ε_e, at the ends as,

$$D_e = \frac{1}{16}\ \frac{\ell^2}{t}\ \varepsilon_e \tag{7}$$

In [9], an irradiation creep modulus, $K = \frac{\varepsilon}{\sigma}$, was substituted into (7) leading to an expression for irradiation induced creep dilation D_i, across opposing flats, where L = linear distance between opposite flats,

$$D_i = .00695\ \frac{\Delta P L^4}{t^3}\ K \tag{8}$$

Total dilation D_t, was obtained by adding dilation from stress-free swelling,

$$D_t = \frac{L}{L+5D_i}\ D_i + \frac{(L+2t)}{3}\ S_o \tag{9}$$

The factor $\frac{L}{L+5D_i}$ was introduced to represent stress relaxation as the duct rounding approached

a cylinder. Our studies with MARC-CDC showed that stress relaxation was negligible at the dilations of interest, so the factor was eventually eliminated in our procedure.

The irradiation creep modulus in this study differed from that in [9] in that it contained a dilatational component. Furthermore, our formulation was based upon a stress and strain state at the hex corner similar to a flat plate. Our derivation of the creep modulus, $\varepsilon_{hoop}/\sigma_{hoop}$, was carried out as follows. The total irradiation induced creep and swelling strain rate tensor ($\dot{\varepsilon}_{ij}$) consists of deviatoric (ε'_{ij}) and dilatational (ε''_{ij}) components.

$$\dot{\varepsilon}_{ij} = \dot{\varepsilon}'_{ij} + \dot{\varepsilon}''_{ij} \qquad (10)$$

From [10], $\dot{\varepsilon}'_{ij} = \frac{3}{2}\frac{\dot{\bar{\varepsilon}}}{\bar{\sigma}}\sigma'_{ij}$ and $\dot{\varepsilon}''_{ij} = \frac{1}{3}\frac{\dot{V}}{V}S_{ij}$ (11a, b)

with $\bar{\sigma} = \sqrt{\frac{3}{2}\sigma'_{ij}\ \sigma'_{ij}}$ and $\dot{\bar{\varepsilon}} = \sqrt{\frac{2}{3}\dot{\varepsilon}'_{ij}\ \dot{\varepsilon}'_{ij}}$ (12a, b)

combining (10), (11), (12) with (4) and (5) and integrating, the hoop strain component is obtained as,

$$\varepsilon_{hoop} = [A(1-\exp(-f/B)) + Cf + DS_o]\ \sigma'_{hoop} + \frac{So}{3}\ (1 + P\sigma_H) \qquad (13)$$

The stress state at the surface of the corner of the hexagonal flow duct is assumed to be a principal stress state with only two non-zero components, σ_{hoop} and $\sigma_{axial} = \nu\sigma_{hoop}$. Under these assumptions,

$$\sigma'_{hoop} = \frac{2-\nu}{3}\ \sigma_{hoop} \text{ and } \sigma_H = \frac{1+\nu}{3}\ \sigma_{hoop} \qquad (14a, b)$$

Substituting (14) into (13), the creep modulus is expressed as,

$$K = \frac{\varepsilon_{hoop} - \frac{S_o}{3}}{\sigma_{hoop}} = [A(1-\exp(-f/B) + Cf + DS_o)]\cdot(1-\tfrac{\nu}{2}) + S_o\ \frac{P(1+\nu)}{9} \qquad (15)$$

Eq. (9), less the stress relaxation factor and including our creep modulus, was programmed to calculate irradiation induced dilation of the flow duct on one inch intervals from bottom to top of the fueled region for the corresponding total damage fluence, duct wall temperature, and pressure at each interval. Input to the program includes maximum damage fluence (core mid-plane), duct wall inlet and outlet temperatures, inlet and outlet differential pressures, duct wall thickness, and inner flat-to-flat distance. Axial profiles of damage fluence, temperature, and pressure (Eqs. 1,2,3) are generated internally by the program. The dilation results are used to evaluate the peak damage fluence, peak burnup, and number of reactor operational cycles that a carbide test assembly can endure in a test location (Row and position) without exceeding the allowable flow duct dilation. As a measure of conservatism, flux, temperature, and pressure characteristics are taken at the beginning of life (BOL) and assumed to remain constant over the life of the test assembly. Also, temperature characteristics of the flow duct are taken for the hex flat with the highest temperature. These conservatisms could be reduced by calculating dilation in increments of reactor cycles, using data characteristic to each cycle.

A final comparison of maximum dilation calculated by the simplified procedure and by MARC-CDC led to modifications of Eq. (9) so that results of the simplified procedure matched those of MARC-CDC.

$$D_t = D_i + \frac{L+2t}{3}\ S_o \qquad \text{(upper bound)} \qquad (16a)$$

$$D_t = 1.05\left[D_i + \frac{L+2t}{3}\ S_o\right] \qquad \text{(nominal)} \qquad (16b)$$

Note that K(15) and $S_o(6)$ would have different values for nominal and upper bound.

6. Nonlinear Finite Element Dilation Analysis

The MARC-CDC finite element program [11] was used for the flow duct dilation analysis [12]. The major difference from the C-E simplified procedure is in the method of computing irradiation induced creep. The MARC-CDC program computes the complete history of non-linear stress distribution across the flat and through the thickness of the hex-flat model and subsequently computes the irradiation induced creep dilation to which is added the swelling dilation. The axial position of maximum dilation calculated by the simplified procedure was confirmed by independent MARC-CDC runs at several axial positions. Although the magnitude of dilation from the simplified procedure was consistently lower than the MARC-CDC results, the fluence dependence and the location of maximum dilation were accurately predicted by the simplified procedure. For a conservative simplification, the core environment at any radial cross section of the duct and the resulting deformation of the duct were assumed to be uniform. This reduces the model to 1/12 of the cross section or one-half of the duct flat (see Figure 4). The two ends of the model were restricted to slide only in the radial direction. The simplified analysis results and typical MARC-CDC runs showed that the magnitude of dilation varied no more than 5% at 2" above and below the axial point of maximum dilation. The situation at the point of maximum dilation is best represented by a generalized plane strain model having uniform strain in the axial direction. The more economical plane strain and plane stress models were tried. The suppressed axial irradiation-induced swelling in the plane strain model induced very high normal stresses. The plane stress model induced high nonuniform normal strain. However, both of these models gave unsatisfactory dilation results. An optimization study led to the choice of the higher order element, type 29. It is a distorted quadilateral with 10 nodes and with each element having 9 integration points. In this element, the in-plane (X,Y) relative displacement is assumed to be a parabolic function and the normal (Z) relative displacement is assumed to vary linearly with X and Y. The basic strain variation in X and Y is assumed to be linear.

The rounded duct corner and the sliding boundary condition required a fine mesh in the corner region of high stresses and high stress gradients. This required a transition mesh between a coarse mesh in the flat region to fine mesh in the rounded corner. Quadrilateral elements and gradual reduction in the element size were incorporated. Triangular transition elements and sharp changes in the element sizes resulted in random stress variation and were unsatisfactory. The input to the MARC-CDC program consisted of core environment parameters and mechanical properties of the duct at the axial position of maximum dilation. Stress and strain tolerances were specified to ensure stable results. The time increments in the nonlinear creep analysis were controlled by the ratio of creep strain change to total strain. The effective stress variation with time, Figure 5, is negligible and hence, is not critical to ensure stable results. The analysis of the 81 element model was repeated with a coarser mesh of 51 elements. It was concluded that although the pressure boundary condition in the rounded corners was not completely satisfied, the ultimate dilation results were unaffected.

The output of program MARC-CDC gave the time history of incremental and total displacements at each node and also the time history of incremental strain, total strain and stress distribution at the 9 integration points of each element. Evaluation of the total displacements perpendicular to the hex-flat showed only swelling dilation at the corner. Maximum creep dilation occurred at the mid-flat. A comparison of the dilation computed by MARC-CDC

and the simplified analysis is shown in Figure 6. The small difference in the swelling component is due to elastic deformation which is neglected in the simplified analysis. A difference in the irradiation-induced creep component is clearly apparent. Agreement was improved by eliminating the assumption of the hex-duct changing to a round duct.

During the course of the dilation analysis, the irradiation induced swelling and creep correlations underwent several revisions. It was suspected at first that the revised correlations could affect the calibration of the creep component and hence the total dilation of the two methods. However, the agreement was found to be consistent. Therefore, factors of 1.0 and 1.05, respectively, were applied to upper limit and nominal values by the simplified procedure.

The MARC-CDC analysis was extended to include the MARK-IB scalloped duct. Except for the geometry and dimensional changes, there is basically no change in the mesh. Although the magnitude of the maximum duct dilation of the scalloped duct was about 8-10% higher than the comparable MARK-IA standard duct, the increase in the allowable dilation typically permits an additional cycle of test. The MARK-IC undersize duct was also investigated with MARC-CDC. Because of its significantly larger allowable dilation, this duct will endure several more cycles of reactor operation, compared to the MARK-IA duct.

The following results show the number of reactor test cycles that the three flow duct designs in FTR Rows 2 and 4 at 680 F inlet temperature will endure without exceeding the maximum flow duct dilation. These calculations are based upon swelling revision 5 and creep revision 3, and conservative assumptions of fluence, temperature and pressure.

	No. of Cycles	
	Row 2	Row 4
MARK-IA	2	3
MARK-IB	3	4
MARK-IC	4	6

7. Above Core Load Pad (ACLP) Structural Evaluation

Because carbide fuel produces a more severe thermal transient on the driver assembly compared to oxide fuel, the MARK-IA ACLP was evaluated for capability to endure six cycles of FTR operation at a 680 F inlet temperature. Loadings on the ACLP over six operational cycles and the number of occurrences were obtained from [2]. The loadings included U1 scram thermal transients (TT), core restraint (CR), seismic events (operating basis earthquake (OBE)), design basis earthquake (DBE), and pressure (P). Thermal analysis of the ACLP during the thermal transient was performed with MARC-HEAT. Stress analysis was performed with the MARC-CDC structural program. Seismic information was obtained from FFTF seismic spectrum response curves [13].

The structural evaluation of the ACLP included analysis for rupture and creep-fatigue material separation failure modes. The results of the stress analysis are shown in Table II, giving the various stress intensities [14] needed for the rupture and creep-fatigue evaluations.

The structural integrity of the ACLP was evaluated by using the elastic analysis criteria of ASME B&PV Code Case 1592-7 [14], supplemented with allowable stresses for CW316SS, given in [15]. The results of the evaluation are summarized in Table III, and show that rupture and creep-fatigue criteria are satisfied for a six FTR cycle design life. The various combined thermal transient, seismic, and core restraint stresses and the total creep-fatigue damage are all 13% or more below the allowables for all loading events.

The reduction in flow duct I.D. to 4.150 in. for the MARK-IC design, without any other changes in assembly design, will result in an ACLP thickness of 0.280 in., compared to the

standard thickness of 0.190 in. A scoping evaluation was performed to estimate the effect of this thickness increase on rupture and creep-fatigue failure criteria. The MARK-IA results were extrapolated to 0.280 in. thickness by ratioing them in proportion to the various geometrical parameters involved in the loading cases. The rupture criterion was satisfied by a greater margin. However, the creep-fatigue criterion was not satisfied for a six FTR cycle design life and was just marginal at four cycles. The design of the MARK-IC ACLP will require further analysis.

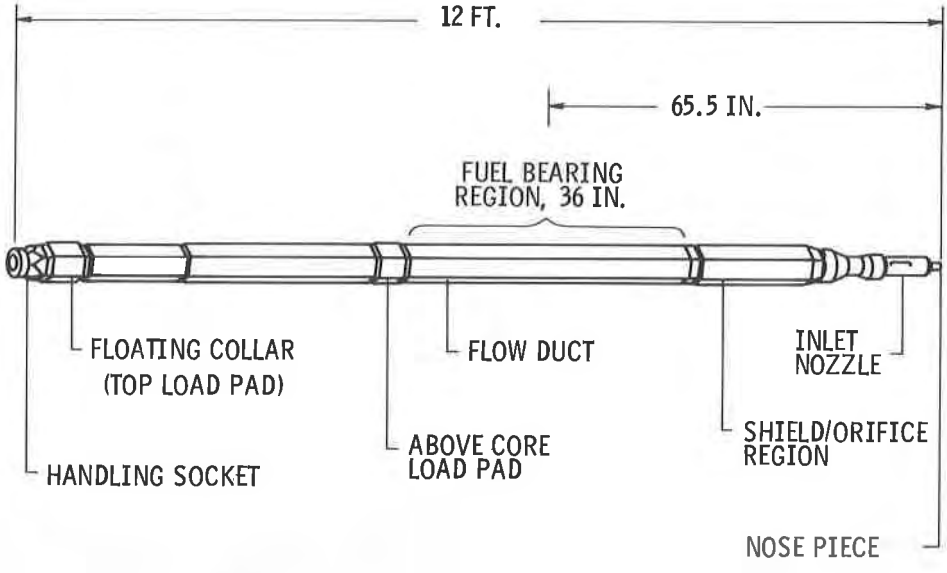

Fig. 1: Standard FTR fuel driver assembly (MARK-IA)

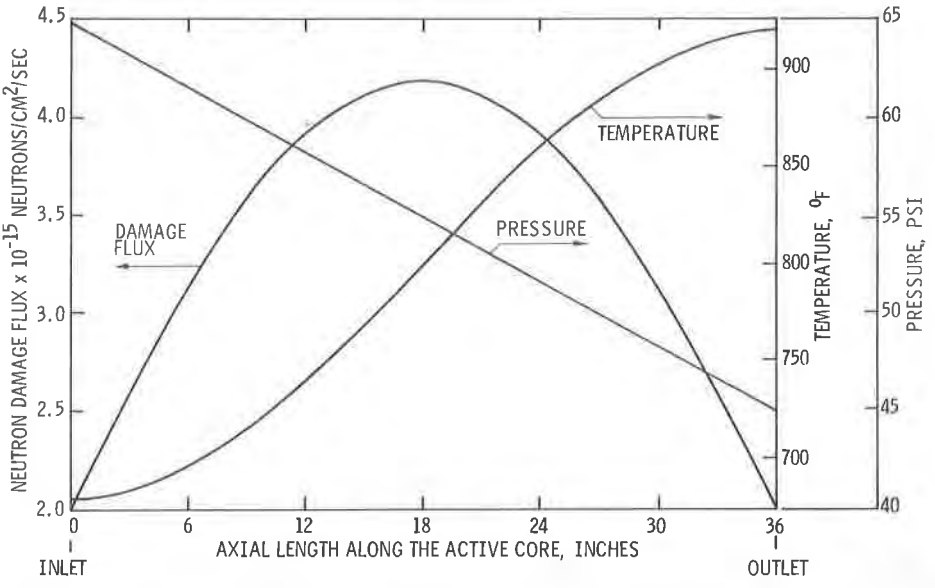

Fig. 2: Typical FTR active core region environment - axial distribution

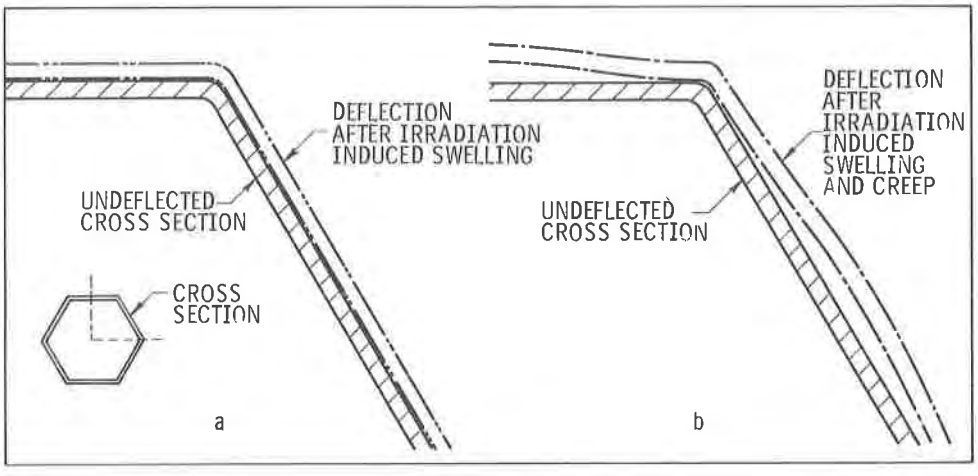

Fig. 3: Irradiation induced flow duct dilation

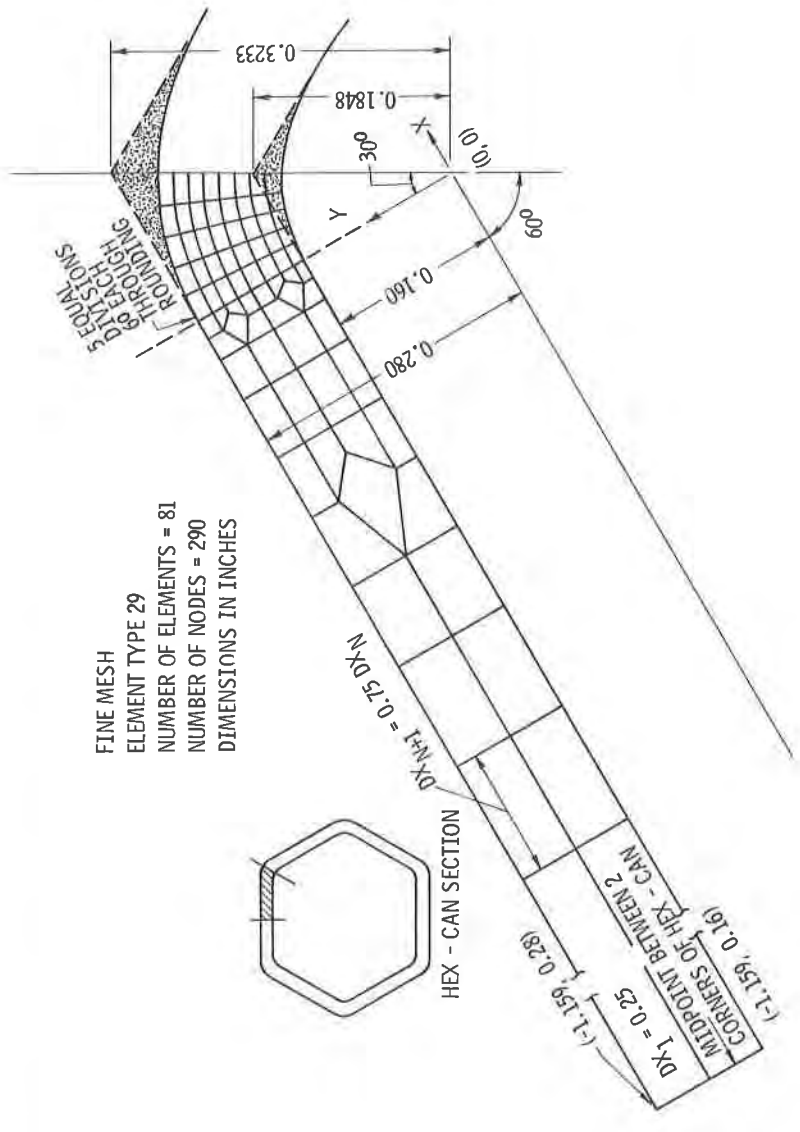

Fig. 4: Flow duct dilation model, MARK-IA

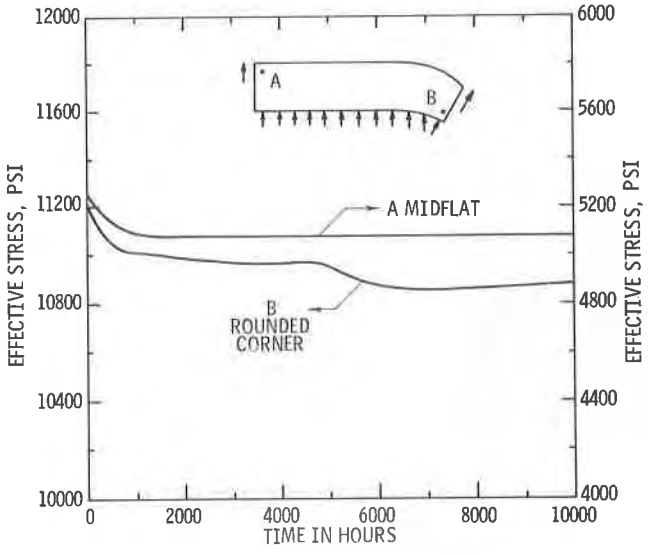

Fig. 5: Effective stress variation with time at midflat and rounded corner (MARK-IA, Row 2, 600 F - 900 F)

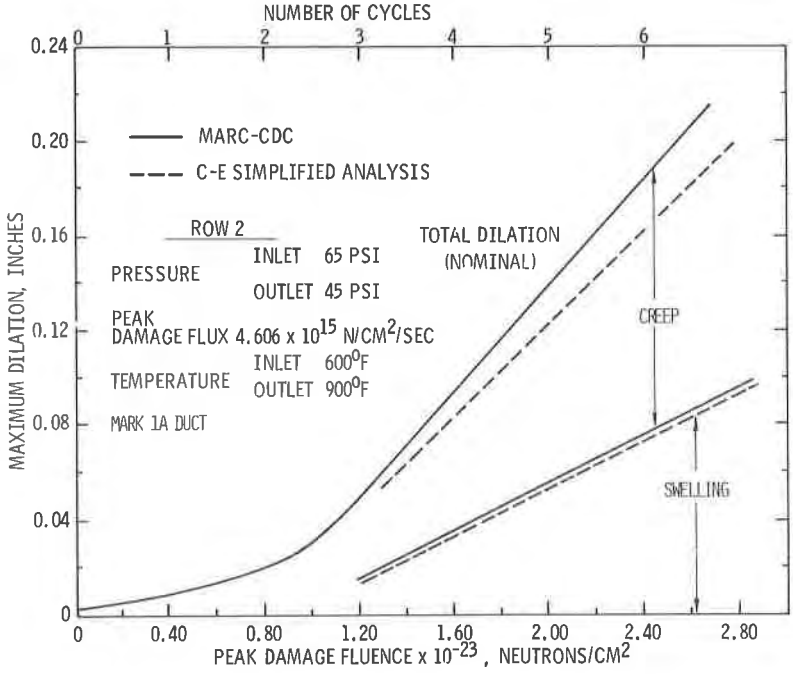

Fig. 6: Comparison of MARC-CDC and simplified analysis dilation

Table I, Flow Duct Designs Evaluated for Carbide Fuel Test Assemblies

Duct Type and Dimensions (in.): MARK-	IA	IB	IC
Outer dimension, flat-to-flat, ACLP	4.715	4.715	4.715
Thickness of ACLP	.190	.190	.283
Outer dimension, flat-to-flat, duct	4.575	4.575	4.390
Inner dimension, flat-to-flat, duct	4.335	4.335	4.150
Duct-duct gap	.140	.214	.325
Thickness of wall	.120	.150	.120
Thickness of wall, mid-flat	.120	.083	.120

Table II, Stress Intensities (psi)

Loading	Primary Local + Bending ($P_L + P_B$)	Primary + Secondary ($P_L + P_b + Q$)	Primary + Secondary + Peak Range ($P_L + P_b + Q + F)_r$
TT	0	26,880	35,470
CR	22,130	22,130	22,130
OBE	5,500	5,500	11,000
DBE	6,870	6,870	13,740
P	1,730	1,730	1,730

Table III, Structural Failure Evaluation of MARK-IA Above Core Load Pad

RUPTURE

EVENT LOAD COMBINATION	ASME EVENT CLASSIFICATION	$P_L + P_B$ (psi)	ALLOWABLE STRESS (psi)	RESULT
P + CR	Normal	23,860	29,800 ($K_t S_t$)	PASS
P + CR + TT	Normal/Upset Emergency	23,860	43,800 (1.5 S_m)	PASS
P + CR + TT + OBE	Upset	29,360	43,800 (1.5 S_m)	PASS
P + CR + TT + DBE	Emergency	30,730	52,600 (1.8 S_m)	PASS

FATIGUE DAMAGE

EVENT LOAD COMBINATION	APPLIED STRESS CYCLES, N	STRAIN RANGE	ALLOWABLE CYCLES, N_d	FATIGUE DAMAGE $(\frac{N}{N_d})$
P + CR	6	$.963 \times 10^{-3}$	14,620	0.0004
P + CR + TT	80	1.83×10^{-3}	197	.406
P + CR + TT + OBE	18	2.27×10^{-3}	96	.188
P + CR + TT + DBE	10	2.38×10^{-3}	90	.111
				.7054

CREEP DAMAGE

EVENT LOAD COMBINATION	TOTAL DURATION, T (HOURS)	$S_K = P_L + P_B + Q$ (PSI)	ALLOWABLE DURATION, T_R (HOURS)	CREEP DAMAGE $(\frac{T}{T_R})$
P + CR	19,437	23,860	3×10^5	0.065
P + CR + TT	2.7	50,740	650	.0042
P + CR + TT + OBE	.1	56,240	197	.0005
P + CR + TT + DBE	.033	57,610	145	.0002
				.0697

TOTAL CREEP PLUS FATIGUE DAMAGE: .705 + .070 = .775 < 1.0 PASS

References

[1] VITTI, J. A. et al, "Design of Prototype Carbide Subassemblies and an Evaluation of Proof-Testing Plans in the FFTF," Nucl. Tech., 26, pp. 442-451 (1975).

[2] Fast Flux Test Facility System Design Description - Reactor System - No. 31.

[3] HEDL MG-22, "User's Guide for the Irradiation of Experiments in the FTR," (July 1975).

[4] VITTI, J. A., Ed., "Preliminary Assessment of Proof Testing LMFBR Carbide Fueled Subassemblies in FTR Driver Positions," ERDA Rpt. No. COO-2465-5 (December 1974).

[5] SIDDALL, W. F., "FTR Carbide Fuel Subassembly Structural Evaluation for Normal Scram Transient," ERDA Rpt. No. COO-2426-23 (July 1975).

[6] DESAULNIERS, W. E., "Structural Evaluation of FTR Carbide Fueled Driver Assembly Above Core Load Pad," (to be published as an ERDA Rpt.).

[7] BHATT, N. R. and DI LAURO, G. F., "Flow and Temperature Distribution Analysis of the FTR Carbide Subassemblies," CE-FBR-76-59 (May 1976).

[8] HEDL TID 26666, Nuclear Systems Materials Handbook, 1, Design Data.

[9] BARTHOLD, W. P., et al, "Breeding Performance and Pin Diameter Optimization for Mixed Carbide and Nitride Fuels in 500 Mwt LMFBR's," Part II, ANL Draft (1974-1975).

[10] CORUM, J. M., et al, "Interim Guidelines for Detailed Inelastic Analysis of High Temperature Reactor System Components," ORNL-5014 (December 1974).

[11] MARC-CDC, "Nonlinear Finite Element Analysis Program," 1,2,3; Rev. G, Rel. 1, Control Data Corp. (March 1975).

[12] MEHTA, D. D., "FTR Carbide Subassembly Flow Duct Dilation," CE-FBR-76-213 & 218 (November 1976).

[13] HWS-1386 (Rev. 7), "FFTF Structure Response Curves for Seismic Design of FFTF Equipment," Bechtel Power Corp. (July 1973).

[14] Code Case 1592-7, "Cases of ASME Boiler and Pressure Vessel Code, Class I, Components In Elevated Temperature Service," Section III (December 1975).

[15] PAXSON, E., "FFTF Fuel Assembly Design Support Document," FRT-1362-Rev. 0, W-ARD (August 1974).

Acknowledgment: This paper was prepared as an account of work sponsored by the United States Energy Research and Development Administration (USERDA).